chemosensors

MDPI

Article

Highly Selective Uricase-Based Quantification of Uric Acid Using Hydrogen Peroxide Sensitive Poly-(vinylpyrrolidone) Templated Copper Nanoclusters as a Fluorescence Probe

Ramar Rajamanikandan [1], Malaichamy Ilanchelian [2] and Heongkyu Ju [1,*]

[1] Department of Physics, Gachon University, Seongnam-si 13120, Republic of Korea; chemistrmkd@gachon.ac.kr
[2] Department of Chemistry, Bharathiar University, Coimbatore 641046, Tamil Nadu, India; chelian73@buc.edu
* Correspondence: batu@gachon.ac.kr

Abstract: We reported on uric acid (UA) detection using a new fluorescence-based assay: poly-(vinylpyrrolidone) templated copper nanoclusters (PVP-CuNCs) with uricase in an aqueous medium, such as human urine with uricase. These nanoclusters were synthesized in a simple wet chemical method and their morphological and optical properties were examined with the aid of high-resolution transmission electron microscopy and optical absorbance/emission spectroscopy. The PVP-CuNCs acted as the fluorescence indicators that used the enzyme-catalyzed oxidation of UA with uricase. Adding UA into the hybrid PVP-CuNCs/uricase solution caused enzyme-catalyzed oxidation to occur, producing hydrogen peroxide (H_2O_2), allantoin, and carbon dioxide. The fluorescence intensity of PVP-CuNCs is decreased by this biocatalytically generated H_2O_2, and this decrease is proportional to the UA level. A calibration plot showed the linear relationship with the negative slope between fluorescence intensity and UA in the range of 5–100 $\times$ 10^{-7} mol/L. The limit of detection (LOD) of UA was estimated as 113 $\times$ 10^{-9} mol/L. This fluorescent probe turned out to be highly specific for UA over other biologically relevant molecules. The demonstrated capability of the PVP-CuNCs as the nanoprobes for quantification of the UA levels in human urine samples could potentially pave the way toward medical applications where a super-sensitive, cost-effective, and UA-specific diagnosis was required.

Keywords: copper nanoclusters; human urine; catalytic oxidation; uric acid detection; uricase; fluorescence

Citation: Rajamanikandan, R.; Ilanchelian, M.; Ju, H. Highly Selective Uricase-Based Quantification of Uric Acid Using Hydrogen Peroxide Sensitive Poly-(vinylpyrrolidone) Templated Copper Nanoclusters as a Fluorescence Probe. *Chemosensors* **2023**, *11*, 268. https://doi.org/10.3390/chemosensors11050268

Academic Editor: Ambra Giannetti

Received: 29 March 2023
Revised: 28 April 2023
Accepted: 28 April 2023
Published: 1 May 2023

1. Introduction

Uric acid (2.6.8-trihydroxypurine, UA), the final product of purine metabolism in the human body, is one of the important biomarkers present in biological fluids such as blood sera and urine [1,2]. Generally, the usual human UA levels in blood sera and urinary secretion are in the range of 240–520 μM and 1.49–4.46 mM, respectively [3]. An unusual UA concentration level has been recognized as a symptom crucial for abnormal metabolic syndromes that increase risks including renal diseases, gout, preeclampsia, diabetes, obesity, and cardiovascular diseases [4–10]. For instance, higher UA concentrations can warn of severe syndromes such as preeclampsia [9], whilst an unusually low concentration indicates risks of sclerosis [11]. This drives the need for a cost-effective, rapid, and simple analytical method for quantifying UA levels in clinical samples for disease diagnosis.

In recent years, several methodological platforms for UA quantification have been developed, such as those by surface-enhanced Raman spectroscopy (SERS) [11], capillary electrophoreses with chemiluminescence [12], matrix-assisted laser desorption/ionization time-of-flight mass spectrometry [13], high-performance liquid chromatography (HPLC) [14], and electrochemical-based methods [3]. Among these approaches, the chromatographic and electrophoretic methods require a piece of sophisticated equipment with complex

sample preparation, while chemiluminescence and electrochemical methods need surface modification and complex electrode construction to improve the recognition specificity.

In contrast, optical methods for UA determination such as colorimetry and fluorometry have gained considerable attention due to simplistic operation procedures, and rapid response [15,16]. Amid optical methods reported, the color change-based colorimetric sensors permit immediate analysis due to naked eyes-based signal readout. Accordingly, metal nanoparticles (MNPs) of various types have been reported as appropriate colorimetric probes for the ultrasensitive detection of UA levels. This is largely due to the high molar optical extinction properties induced by the localized surface plasmon, with its resonance varying with both the particle size and local index change [17–19]. However, the MNP-based color indicators can be interfered with by the local compound matrix coated around them, which would be a prerequisite for surface functionalization [15].

Meanwhile, one of the widely used optical methods suitable for analytical diagnosis relies on fluorescence-based sensing platforms, owing to the ultra-high sensitivity, rapid sensor response, and relatively low cost of operation [20–24]. The key factors to this platform mostly reside in the fluorescent probe to which the sensing selectivity and sensitivity are inherently subject.

Researchers have thus paid considerable attention to numerous noble metal nanoclusters as fluorescent probes, including those of Cu, Ag, and Au, due to their excellent electronic and optical features [25–28]. In particular, the fluorescent Cu nanoclusters (CuNCs) have been studied continually owing to their quite low cost, wide availability, good water solubility, and fluorescence tunability [26,27]. These advantages have led to a wide range of their applications [28], despite their easy oxidation and labor-intensive synthesis. Recently, numerous literatures have reported that synthesis of the fluorescent CuNCs is possible for multifunctional uses with various fluorescence tunability, photostability, and biocompatibility [29–32]. Due to their low harmfulness and ultra-fine dimensions, the CuNCs have been developed as capable applicants for catalysts, molecular bio-imaging, and bio-chemo sensors [33–37]. To date, use of the CuNCs for diagnostic sensing has been primarily focused on their emissive features associated with catalytic activity [34,36]. Most fluorescence-based analytical tactics with CuNCs have employed their emission modulation such as the turn-on/off by analyte influence through fluorophore–analyte interfaces.

In this study, we present the hydrogen peroxide (H_2O_2)-induced emission quenching method based on poly-(vinylpyrrolidone) (PVP)-stabilized CuNCs (PVP-CuNCs) as effective fluorophores for the detection of UA. The uricase-catalyzed oxidation of uric acid produces H_2O_2, consequently interfering the emissive nature of PVP-CuNCs (Scheme 1). We find that the catalytic reaction-based fluorometric methods offer highly specific and sensitive determination of UA in clinical specimens, including human urine samples with satisfactory recoveries (relative standard deviation (RSD) < 3%). The proposed method shows a linear response in a quite broad range of $5-100 \times 10^{-7}$ mol/L for the quantitative sensing with the LOD estimated as 113×10^{-9} mol/L. This feature would lend itself to the convenient application of a clinical assay while opening the potential application for other clinical tests using different enzymes.

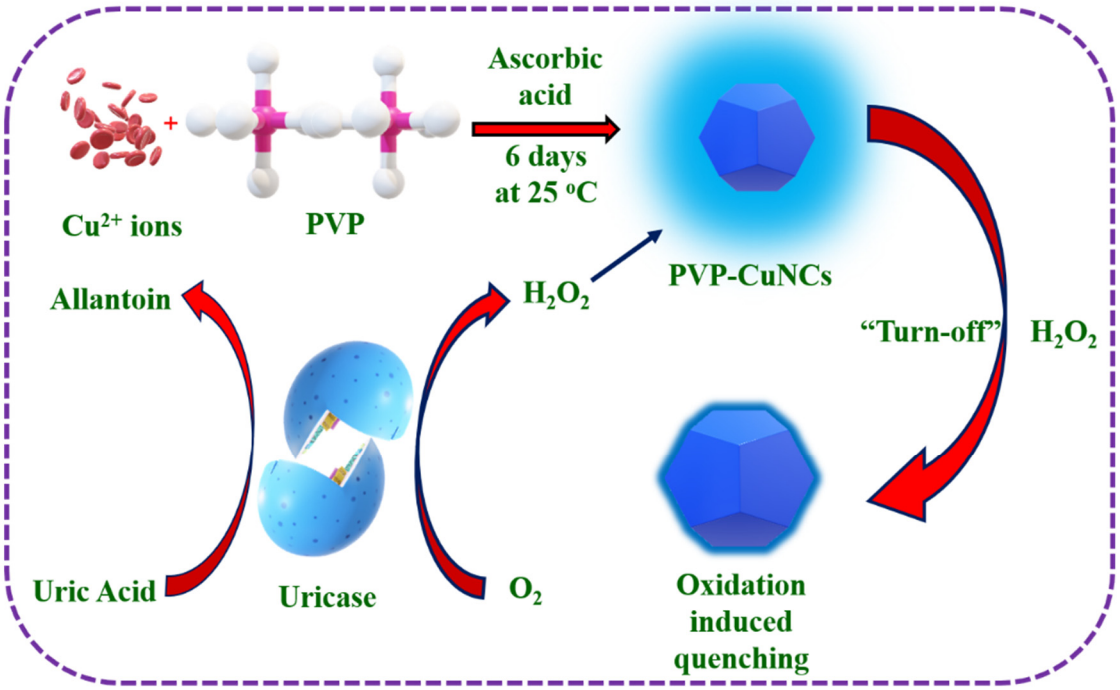

Scheme 1. Schematic for oxidation of UA with uricase, followed by the H_2O_2-induced emission quenching of PVP-CuNCs.

2. Experimental Design

2.1. Reagents

Uricase, uric acid, PVP (molecular weight, ~40 kDa), ascorbic acid (AA), dopamine (DA), glutathione (GSH), adenine (Adn), guanine (Gua), thymine (Thy), and cytosine (Cyt) were purchased from Sigma Aldrich, Rahway, USA (http://www.sigmaaldrich.com/ (accessed on 1 September 2019)). Glucose (Glu) and copper sulfate pentahydrate were obtained from Merck. Cysteine (Cys), sodium hydroxide (NaOH), H_2O_2, and sucrose (Suc) were purchased from Loba Chemie Private Limited, Mumbai, India. All reagents used were of a minimum analytical reagent grade and used without any purification. The stock solution of UA prepared using a certain quantity (17 mg) of UA salt was dissolved in a few drops of 1 M NaOH, fixed in phosphate buffer saline (PBS) (10 mM, pH 7.5), and stored at 5 °C in a refrigerator. All related investigations were three times repeatedly conducted at a minimum under ambient conditions.

2.2. Instruments

Ultraviolet (UV)-visible absorbance spectral data were taken by a spectrophotometer (V-630, JASCO, Tokyo, Japan) in the 800–200 nm range. Fluorescence spectral studies (both emission and excitation) were performed using a spectrofluorometer (JASCO FP-6600, Tokyo, Japan) with a spectral resolution of ~1 nm. High-resolution transmission electron microscopic (HR-TEM) images of nanostructured PVP-CuNCs were taken by an instrument (JEOL JEM 2100 HR-TEM, Ltd., Tokyo, Japan) with a voltage of 200 kV. For HR-TEM analysis, the sample was prepared by dropping 2 µL of a PVP-CuNCs colloidal solution onto a carbon-coated copper grid and drying it in the air. Dynamic light scattering (DLS) data for PVP-CuNCs were taken using an instrument (Zetasizer Nano ZS) with a 633 nm He−Ne laser, equipped with an MPT-2 auto-titrator (Malvern, UK). Fluorescence lifetime experiments were performed using a time-correlated single photon counting fluorometer (Horiba Scientific, Kyoto, Japan) with an NL-C2 throbbed diode excitation source at 380 nm.

2.3. Synthesis of the PVP-Decorated CuNCs

PVP-decorated CuNCs were synthesized as previously described [38,39]. The synthetic protocol of the PVP-decorated CuNCs was displayed in Scheme 1. PVP of 0.5 g was added to the water of 10 mL. The mixed suspension then was sonicated for 10 min and the pH of the medium was altered to ~6.0 using 1 mol/L of NaOH. Then, $CuSO_4 \cdot 5H_2O$ (0.1 mol/L) of 100 µL and AA (0.1 mol/L) of 1 mL were stirred with the PVP aqueous suspension, followed by a reaction for 6 days at room temperature (25 °C), which produced a slightly yellow suspension. The colloidal dispersion displayed a cyan-blue color under a UV light (λ = 365 nm), which undoubtedly confirmed the construction of PVP-decorated CuNCs. Lastly, the PVP-CuNCs were dialyzed using distilled water and kept at 5 °C in a refrigerator for further characterization and applications.

2.4. Characterization of the PVP-CuNCs

An easy one-pot protocol was applied to synthesize the PVP-CuNCs using $CuSO_4 \cdot 5H_2O$ as predecessors, the AA as a reducing agent, and the PVP as a surface functionalizing ligand (Scheme 1). The PVP was selected as the surface stabilizing and capping ligand owing to its solubility in water, remarkable stabilizing ability, and biodegradability [38,39]. Properties of the PVP-CuNCs were investigated using optical absorbance spectroscopy, the DLS, the HR-TEM, and the time-resolved fluorescence spectroscopic studies. In Figure 1, the absence of plasmon resonance-induced absorbance resonance in the range of the visible wavelength (400–800 nm) indicated the development of the nanoclusters over which significant Ohmic loss of energy lowered the quality factor (Q-factor) due to their extremely small size (no plasmon formation) [19,23]. In daylight, the PVP-CuNCs appeared yellow (inset of Figure 1i).

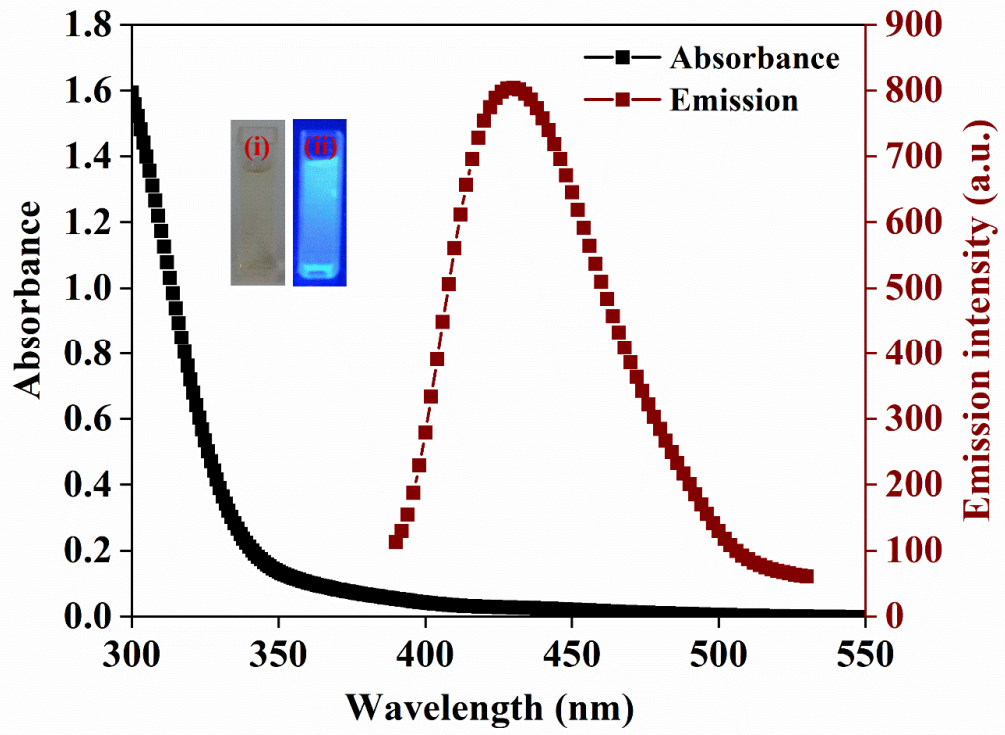

Figure 1. The absorbance and fluorescence (emission) spectra of the as-prepared PVP-CuNCs. The inset shows a photo of a cuvette cell containing the PVP-CuNCs under daylight (**i**) and the illumination of UV light (**ii**) spectrally centered at λ = 365 nm.

Fluorescent properties of the PVP-CuNCs were examined via photoluminescence spectroscopy, as shown in Figure 1. The PVP-CuNCs exhibited the fluorescence peak at 429 nm under an excitation light source spectrally centered at the wavelength of 382 nm.

The PVP-CuNCs colloidal dispersion was slightly yellow colored. Its color turned to a bright cyan-blue color under the illumination of UV light at a wavelength of 365 nm, due to its photoluminescence (inset of Figure 1ii). Similar kinds of fluorescent behavior of CuNCs were reported previously [38,39].

HR-TEM images were taken for the morphology of the PVP-CuNCs as shown in Figure 2. As seen in Figure 2, the PVP-CuNCs were reasonably uniform in size, somewhat spherical in shape, and mono-dispersed, while having an average diameter of approximately 2.8 ± 0.3 nm, even in the presence of the surface-protecting layer of PVP molecules. These HR-TEM findings clearly indicated the formation of PVP-coated CuNCs. The average diameter of PVP-CuNCs in an aqueous medium was investigated by DLS studies, and the collected results were given in Figure S1. DLS results revealed that the PVP-CuNCs possessed an average diameter of approximately 5 nm (Figure S1). PVP-CuNCs particle size determined by DLS measurements slightly differed from that determined via HR-TEM investigation (Figure 2). The HR-TEM study was also performed with samples in the dried phase, therefore avoiding misrepresentation of the particle size possibly induced by the solution phase. The particle size variation of DLS data was used to depict the hydrodynamic diameter of a sphere or the diameter of a particle with a hydration shell, the same volume as the particle, and the extra solvent or stabilizer moving with the particle [40].

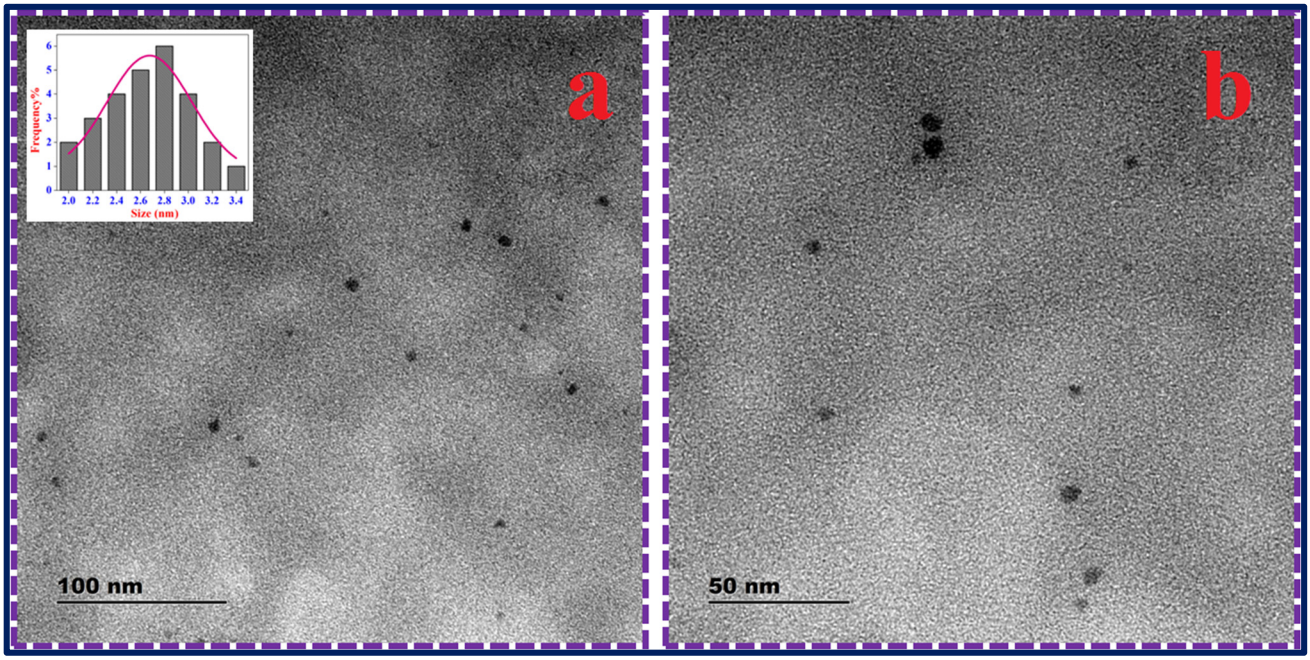

Figure 2. HR-TEM images (**a**,**b**) of PVP-CuNCs at different magnifications. The inset in (**a**) shows the size distribution of PVP-CuNCs.

2.5. General procedures for Detecting H_2O_2 and UA

To substantiate the tenability of this method, we first focused on the direct quantification of H_2O_2 using the following steps. First, different amounts of H_2O_2 analyte (in the range of 4–80 × 10^{-7} mol/L) were mixed with a PBS (pH 7.5) colloidal solution containing the PVP-CuNCs of 100 µL. Then, this reaction mixture was made to react for 15 min at room temperature. The emission spectra studies were carried out in the wavelength range of 390–510 nm with the excitation light wavelength of 382 nm.

On the other hand, the detection of UA levels in PBS took the following steps. Initially, UA solutions in concentrations ranging from 5 to 100 × 10^{-7} mol/L were incubated with uricase of 10 mg/mL (selected after optimization) in PBS (pH 7.5) of 3 mL at ~35 °C for half an hour to produce H_2O_2. Next, the PVP-CuNCs colloidal solution of 100 µL was mixed with the uricase UA solution and the mixture was made to react for 15 min at room

temperature. Emission spectral data were taken with an excitation light wavelength of 382 nm. The same procedures mentioned above were also applied for the selectivity experiment for which other interfering substances in the mixture replaced UA. The analytical use of the developed method was assessed by adding UA at two different concentrations to the two urine samples and analyzing the amounts recovered. The recovery amounts (%) was calculated as the proportion between the volume of spiked and identified UA. It was estimated [19,24,40] according to the following equation (Equation (1)):

$$\text{Recovery } (\%) = \frac{Amount\ of\ UA\ added}{Amount\ of\ UA\ found} \times 100 \quad (1)$$

3. Results and Discussion

3.1. PVP-CuNCs-Based Fluorescence Detection of H_2O_2

It is known that H_2O_2 is usually a side product of the enzyme-catalyzed oxidation of the corresponding substrates by an O_2-dependent oxidase [41,42]. H_2O_2 is involved in various biological, chemical, environmental, and pharmaceutical developments. In this study, we utilized PVP-modified CuNCs for the determination of H_2O_2. When the generated H_2O_2 molecules are in proximity to the PVP-CuNCs, they quench the fluorescence that the PVP-CuNCs emit, due to the following oxidization processes of CuNCs [41,43,44]:

$$Cu^0 + 2H_2O_2 \rightarrow Cu^+ + O_2^- + 2H_2O, \quad (2)$$

$$Cu^0 + H_2O_2 \rightarrow Cu^+ + \dot{O}H + OH^-, \quad (3)$$

$$Cu^+ + H_2O_2 \rightarrow Cu^{2+} + \dot{O}H + OH^-, \quad (4)$$

$$\dot{O}H + H_2O_2 \rightarrow O_2^- + 2H_2O + H^+. \quad (5)$$

Oxidation of the CuNCs leads to the degradation of the NCs, reducing the fluorescence [43]. The fluorescence-quenching properties can thus be used to quantitatively determine the concentration of H_2O_2. As shown in Figure 3a, a rise in the H_2O_2 concentration gradually reduced the fluorescence intensity of PVP-CuNCs. Figure 3b shows the nearly linear plot for the fluorescence spectral peak intensity versus a concentration of H_2O_2 in the H_2O_2 range of 0–80 $\times$ 10^{-7} mol/L. The linear fit to data with $R^2 = 0.993$ indicated that the PVP-CuNCs could be used as the fluorescence-based nanoprobes to quantify H_2O_2 concentration (Figure 3b). We used the definition of the limit of detection (LOD) given by the International Union of Pure and Applied Chemistry (IUPAC) criteria, i.e., LOD = 3 S/m where S denoted the standard deviation of the signal at blank sample and m denoted the slope of the calibration curve. The LOD of the PVP-coated CuNCs-based detection of H_2O_2 was estimated to be 91 $\times$ 10^{-9} mol/L, the concentration corresponding to three times the blank signal (no H_2O_2 case), being much smaller than those obtained with BSA-silver/gold NCs or gold NCs [22,45]. PVP-coated CuNCs-based nanoprobes can also serve as a potential fluorescence platform for determining several other species involved in the creation of H_2O_2 in various biological substrates.

Generally, the emission quenching data are analyzed by the conventional Stern–Volmer equation (Equation (6)) [46,47]

$$\frac{F_0}{F} = 1 + k_{sv}[Q] \quad (6)$$

where, F_0 and F are the emission intensity of PVP-CuNCs before and after the addition of H_2O_2, respectively; $[Q]$ and k_{sv} are the concentration of H_2O_2 and Stern–Volmer quenching constant, respectively. The Stern–Volmer plot F_0/F versus the concentrations of H_2O_2 is shown in Figure S2. The found Stern–Volmer plot had a good linear fit in the range from 0.4 to 4.8 µM and k_{sv} was found to be 1.67 $\times$ 10^5 L mol^{-1}. The positive deviation was noted at

high concentrations of H_2O_2 (Figure S2). This might be caused by the coexistence of static and dynamic quenching [46,48]. The calculated Stern–Volmer constant value indicates that PVP-CuNCs and H_2O_2 exhibit substantial fluorescence quenching.

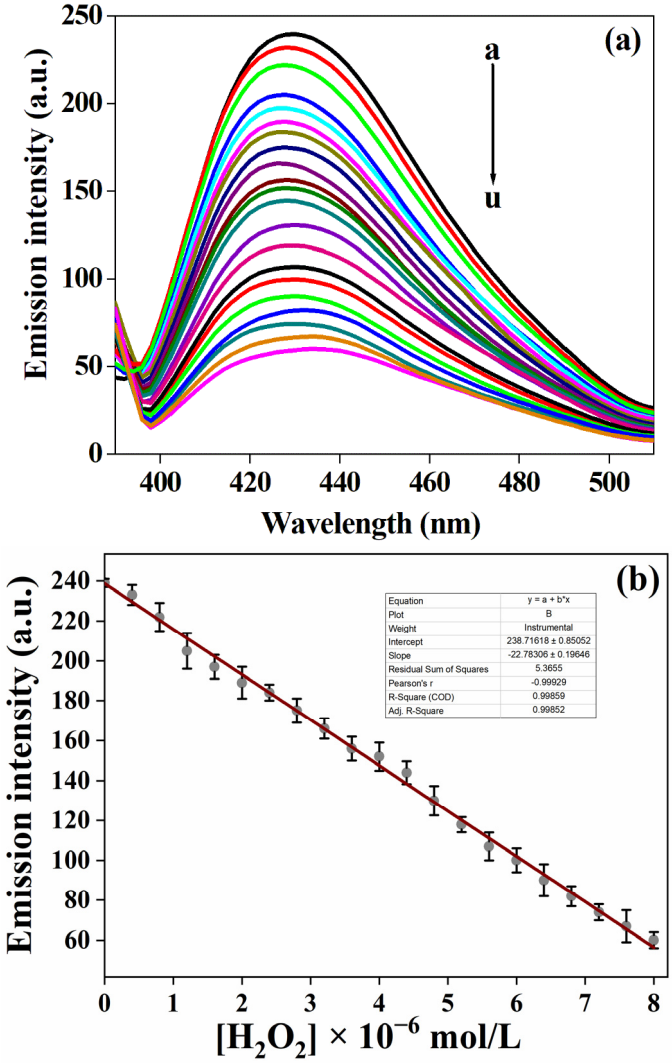

Figure 3. (**a**) Fluorescence spectra of the PVP−CuNCs at various concentrations of H_2O_2 ranging from 0 to 80 × 10^{-7} mol/L (incremental step of 4 × 10^{-7} mol/L). (**b**) A linear fit to data of the peak intensities of emission spectra versus H_2O_2 concentration.

The observable emission quenching of the PVP-templated CuNCs with H_2O_2 was due to the oxidation of CuNCs, which led to the NCs degradation and blocked the ligand-to-metal charge transfer of the CuNCs [43]. To verify the hypothesis, a HR-TEM image and time-resolved fluorescence signals of PVP-CuNCs with H_2O_2 were taken and typical results are given in Figure S3 and Figure S4, respectively. From Figure S3, the HR-TEM image of PVP-CuNCs with H_2O_2 showed no presence of the NCs morphology, indicating the H_2O_2-induced degradation of the CuNCs. Meanwhile, the time-resolved fluorescence (decay profile) showed a shorter lifetime for the PVP–CuNCs with H_2O_2 (1.85 ns) than that without H_2O_2 (3.45 ns), as shown in Figure S4. The H_2O_2-induced blocking of charge transfer from ligand to NCs shortened the lifetime, similar to the previous reports [49,50].

3.2. Optimization for the Detection of UA by PVP-Coated CuNCs

We first optimized the analytical parameters involving the pH, the incubation time for uricase-based catalytic reactions, the buffer solution type, and the uricase concentra-

tion. Figure 4a illustrated that the UA of 1.0 μM induced the reduction in fluorescence emitted from PVP-CuNCs over the pH ranging from 7.0 to 8.5. The maximum fluorescence difference (reduction) took place at the pH of 7.5, which coincided with that of a typical physiological state. The 7.5 pH was used for the UA detection optimization.

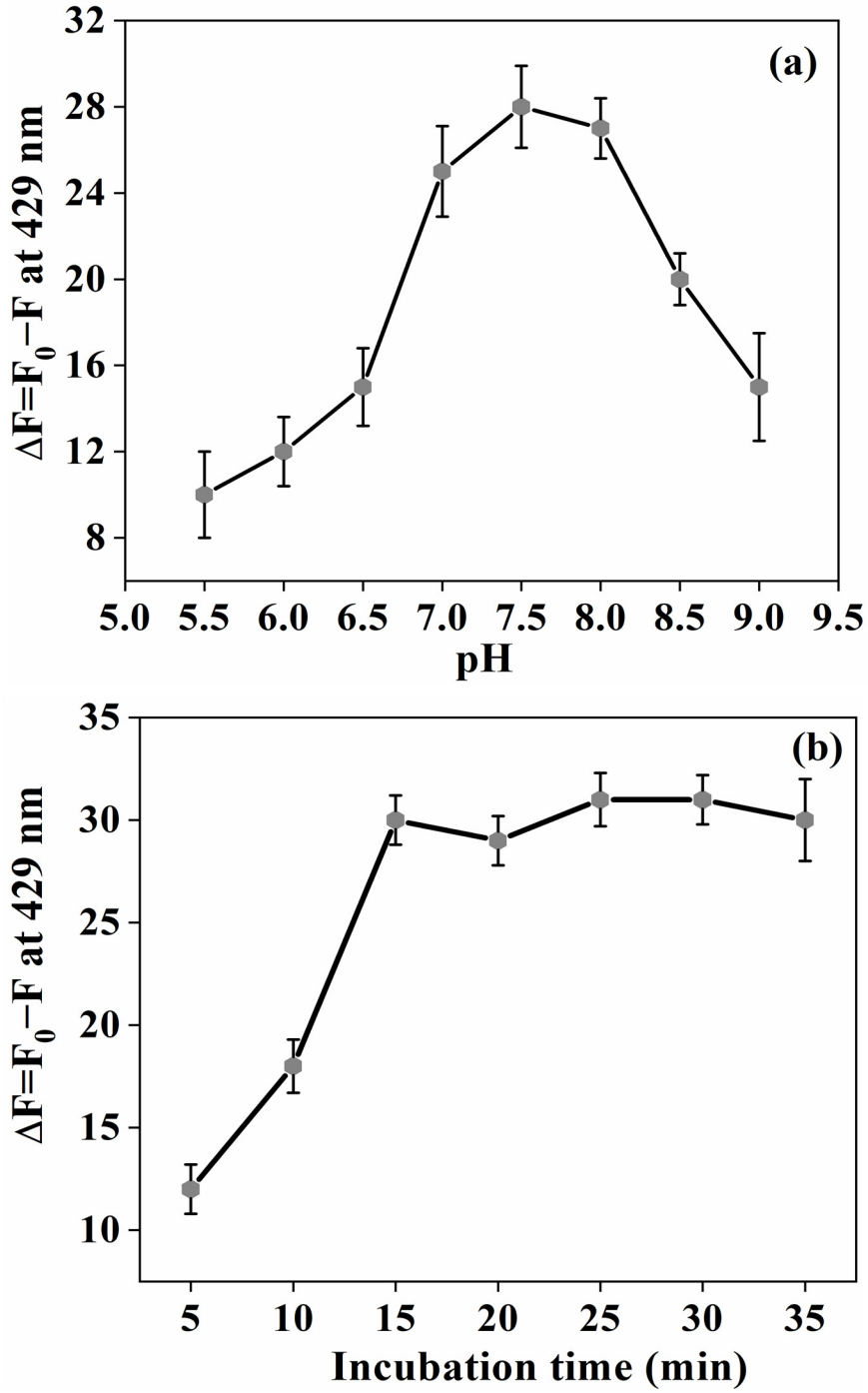

Figure 4. Effects of the pH (**a**) and incubation time (**b**) on UA-induced fluorescence quenching. The F_0 and the F are the fluorescence intensities at the peak wavelength of 429 nm without and with UA (1.0 μM), respectively. Error bars were estimated from three replicate measurements.

Furthermore, we verified the effects of various types of buffer solutions (10 mM, pH 7.5) on UA-induced fluorescence quenching, such as the PBS, the Tris-HCl, and the Tris-acetate. Amid those buffer solutions, the maximum quenching efficacy of fluorescence was obtained with the PBS (10 mM, pH 7.5) solution in case of using a UA level of 1.0 μM

(Figure S5). Thus, this buffer was adopted for quenching optimization. We also examined the effects of the incubation time on UA(1.0 μM)-induced fluorescence quenching with the PBS (10 mM, pH 7.5) solution. Quenching reached its saturation at the incubation of 15 min (Figure 4b), being adopted for optimizing the assay of quenching-based detection of UA.

Lastly, we investigate the influence of a uricase concentration on UA(1.0 μM)-induced fluorescence quenching. We varied the concentration of uricase for optimizing fluorescence quenching at the analytical conditions that had been pre-optimized including the buffer solution of PBS (10 mM, pH 7.5) and the incubation time of 15 min. The uricase concentration of 10 mg/mL^{-1} turned out to yield the maximum efficacy of fluorescence quenching, as shown in Figure S6. This concentration of uricase was then adopted to optimize fluorescence quenching when UA levels finally were assayed.

3.3. Enzymatic detection of UA by the PVP-CuNCs

The above-mentioned PVP-coated CuNCs with their fluorescence sensitivity to H_2O_2 could thus find an application in screening catalytic processes that produce H_2O_2 via an enzyme for biocatalytic oxidation of substrates. Particularly, the fact that oxidation of UA with the enzyme (uricase) generates the products of CO_2, allantoin, and H_2O_2 (Scheme 2) [50,51] could lead us to use PVP-coated CuNCs as fluorophore probes for detecting UA levels.

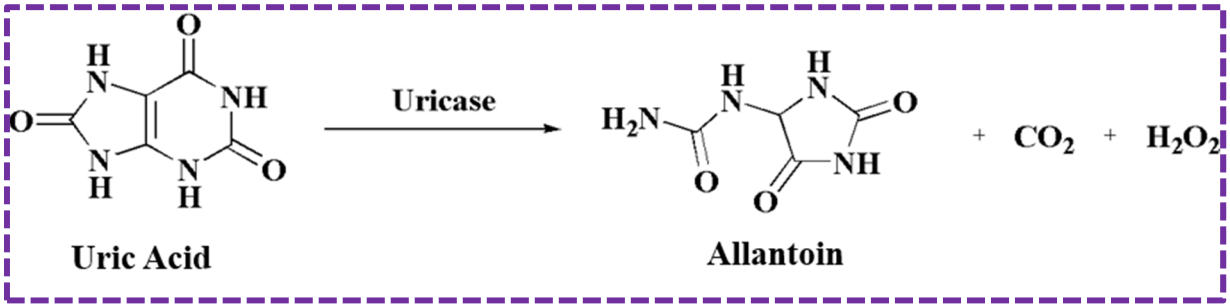

Scheme 2. Biocatalytic oxidation of uric acid in the presence of uricase.

With all the above-mentioned analytical parameters adopted for optimization, final assays of various UA concentrations were conducted as shown in Figure 5a. The absence of injected UA produced the fluorescence spectrum, its peak intensity serving as the starting point from which, when UA was injected, the peak intensity reduced due to UA-induced fluorescence quenching [50,51]. With increasing UA concentration from 0.5 to 10 μmol/L (incremental step of 0.5 μmol/L), the fluorescence signal decreased due to the generated H_2O_2 that resulted in oxidization of the PVP-coated CuNCs. Figure 5b shows the linear relationship between the reduction in the fluorescence spectral peak intensity and the UA concentration, with its linear fit supporting the accurate quantitative detection of unknown UA levels in human urine samples. The LOD of UA was determined as 113×10^{-9} mol/L with a detection range of $0.5-10 \times 10^{-6}$ mol/L. As seen in Table 1, the presented results showed a reasonably broad range of UA detection and the LOD comparable or smaller than those previously reported via fluorescence-based assays of UA levels with nanostructured materials [22,50,52–60]. It was worthwhile to note that the presented strategy did not necessitate covalent cross-linking of uricase, allowing the enzyme-catalyzed oxidation to remain undisturbed and ensuring ease of operation for the quantification of UA.

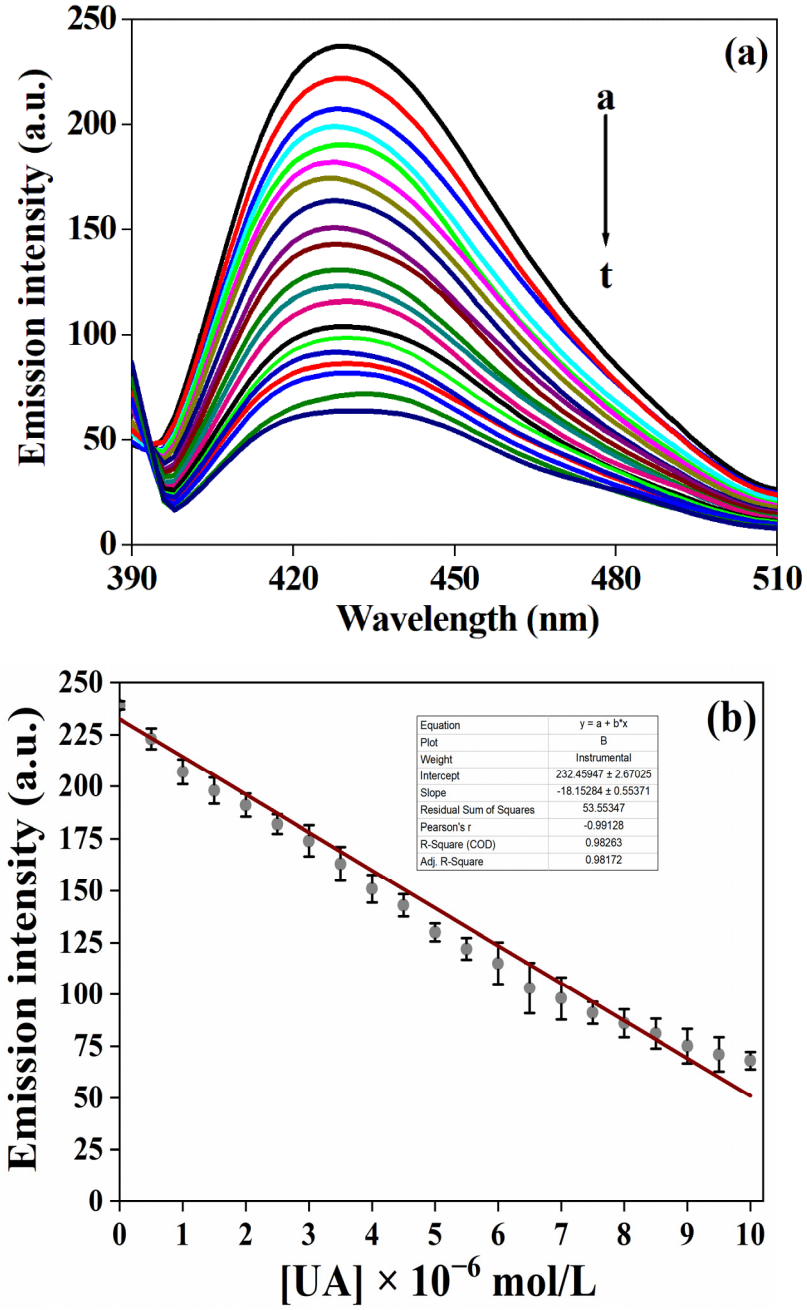

Figure 5. (**a**) Fluorescence spectra of the PVP-CuNCs/uricase with increasing UA concentration ranging from 0.5 to 10 µmol/L (step of 0.5 µmol/L), and (**b**) the fluorescence spectral peak intensity versus the UA concentration in PBS (pH 7.5) uricase = 10 mg/mL.

3.4. Specificity of the Present Assay

The capability of determining the UA specifically is critically important, given various molecules that possibly interfere with the right quantification of the target in human excretion. We tested the specificity by mixing possibly interfering elements such as KCl, NaCl, DA, Glu, Adn, GSH, Cys, Gua, Thy, Suc, Cyt, and AA. For the specificity test, we added each possibly interfering element such as DA, Glu, Adn, GSH, Cys, Gua, Thy, Suc, Cyt, and AA of 5-fold higher concentration than UA one. Figure 6 shows the fluorescence quenching magnitude $\Delta F = F_0 - F$ where F_0 and F represent the quenching with and without an analyte (one of such interfering elements and the UA), respectively. Encouragingly, the addition of only the UA induced quenching substantially whereas the other elements induced negligible quenching. This also manifested that the side product of the enzyme-

catalyzed reaction, i.e., H_2O_2 caused oxidation of the CuNCs, leading to blocking the ligand-to-metal charge transfer.

Table 1. Analytical performance of various fluorescence methods involving nanostructured materials for UA detection.

Method	Materials	Linear Range	Detection Limit	Ref.
Fluorescence	BSA-Ag/AuNCs	5–50 μM	5.1 μM	[16]
Fluorescence	BSA-AuNCs	10–800 μM	6.6 μM	[50]
Fluorescence	Graphene QDs-Ag nanocomposite	5–500 μM	2 μM	[52]
Fluorescence	S, N-co doped carbon dots	0.08–10 μM	0.07 μM	[53]
Fluorescence	Ti_3C_2 Mxene QDs	1.2–75 μM	125 nM	[54]
Fluorescence	N doped carbon dots	0.5–150 μM	60 nM	[55]
Fluorescence	Cadmium sulfide QDs	125–1000 μM	125 μM	[56]
Fluorescence	Chondroitin sulfate-AuNCs	5–100 μM	1.7 μM	[57]
Fluorescence	Cadmium sulfide QDs	60–2000 μM	50 μM	[58]
Fluorescence	Cadmium tellurium QDs	0.2–6 μM	0.1 μM	[59]
Fluorescence	Carbon dots@ZIP-CuNCs	1–100 μM	0.3 μM	[60]
Fluorescence	**PVP-CuNCs**	**0.5–10 μM**	**113 nM**	**This work**

BSA–Bovine serum albumin. QDs–Quantum dots. N–Nitrogen. S–Sulfur.

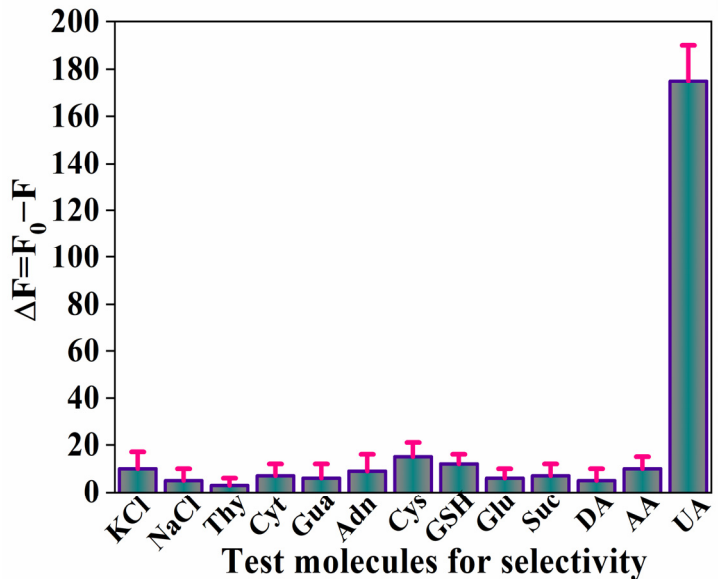

Figure 6. A bar diagram demonstrating the specificity of the UA assay based on fluorescence quenching of the PVP-CuNCs in the presence of KCl, NaCl, UA, DA, Glu, Adn, GSH, Cys, Gua, Thy, Suc, Cyt, and AA in PBS (pH 7.5). The quenching magnitude is denoted by $\Delta F = F_0 - F$ where the F_0 and F represent the fluorescence spectral peak intensities with and without an analyte (one of such interfering elements and the UA), respectively. The concentration of biochemical elements tested (except the UA) was 5-fold higher than UA. Error bars were estimated from three replicate measurements.

3.5. Analytical Application of the Present Fluorescence Platform

To examine the applicability of the presented fluorescence platform for quantitative detection of UA levels in clinical samples, we attempted to detect the UA levels in human urine samples using the standard addition method. Two different UA concentrations were spiked into urine samples with the PVP-CuNCs and uricase in PBS (pH 7.5). We estimated the recovery at each urine sample as shown in Table 2. The recoveries were all above 96% (accuracy) with relative standard deviations of less than 3% (precision). The observed outcomes clearly showed the great clinical applicability of the presented assay to quantitative detection of UA levels in human urine samples with satisfactory accuracy and

precision. Therefore, the present fluorescence-based assay could be considered a promising candidate for clinical use.

Table 2. Analytical data of hybrid PVP-CuNCs/uricase with UA in human urine samples.

Samples	Average Found ($\times 10^{-6}$ mol/L)	Spiked ($\times 10^{-6}$ mol/L)	Calculated ($\times 10^{-6}$ mol/L)	Recovery (%)	RSD (n = 3)
Urine sample 1	0.158	3.00	3.098	98.12	2.3
		6.00	6.013	97.67	1.7
Urine sample 2	0.183	3.00	3.107	97.61	1.5
		6.00	5.965	96.86	2.8

RSD: Relative standard deviation.

4. Conclusions

We demonstrated the fluorescence-based detection of UA concentration in an aqueous medium such as human urine, using PVP-coated CuNCs with uricase. The injected UA molecules chemically interacted with PVP-coated CuNCs and then generated H_2O_2, which subsequently oxidized CuNCs, leading to fluorescence quenching due to blocking ligand–metal charge transfer. This quenching nature enabled us to quantify H_2O_2 in the range of 4–80 $\times$ 10^{-7} mol/L with an LOD of 91 $\times$ 10^{-9} mol/L. This H_2O_2-sensitive nanoprobe was applied to detect the catalytic oxidation of UA with uricase, permitting UA to be quantified in the range of 5−100 $\times$ 10^{-7} mol/L with the LOD of 113 $\times$ 10^{-9} mol/L.

The experimental outcomes clearly validated that a PVP-CuNCs-based fluorescence platform can be applied as a sensitive and excellently specific assay of UA in clinical samples such as human urine. The added enzyme amount in the reaction mixture enhanced the specificity of this assay. In addition, the use of water/buffer dispersible PVP-coated CuNCs that are relatively non-toxic, biocompatible, and straightforwardly synthesizable could accelerate the application of the presented nanoprobe technology to the clinical assay with high specificity and sensitivity. Given these advantages, the present highly fluorescent CuNCs-based assay can be effectively applied in clinical applications.

Supplementary Materials: The following are available online at https://www.mdpi.com/article/10.3390/chemosensors11050268/s1, Figure S1: The DLS results for the PVP-CuNCs. Figure S2: A HR-TEM image of PVP-CuNCs in the presence of H_2O_2 of 7.5 μM. Figure S3: The temporal decay profile of the PVP-CuNCs fluorescence in the presence of H_2O_2 of 7.5 μM. Figure S4: Effects of the pH on UA-induced fluorescence quenching. The F_0 and the F are the fluorescence intensities at the peak wavelength of 429 nm without and with UA (1.0 μM), respectively. Error bars were estimated from three replicate measurements. Figure S5: Effects of the buffer kind on UA-induced fluorescence quenching. The F_0 and F are the fluorescence intensities at the peak wavelength of 429 nm without and with UA (1.0 μM), respectively. Error bars were estimated from three replicate measurements. Figure S6: Effects of the incubation time on the UA-induced fluorescence quenching. The F_0 and F are the fluorescence intensities at the peak wavelength of 429 nm without and with UA (1.0 μM), respectively. Error bars were estimated from three replicate measurements. Figure S7: Effects of the UA-induced fluorescence quenching on uricase concentration. The F_0 and F are the fluorescence intensities at the peak wavelength of 429 nm without and with UA (10 μM), respectively. Error bars were estimated from three replicate measurements. Table S1: Analytical performance of various fluorescence methods involving nanostructured materials for UA detection.

Author Contributions: R.R.: Conceptualization, Methodology, Data Curation, Formal analysis, Investigation, Writing-Original Draft. M.I.: Validation, Investigation, Resources, Visualization, Writing-Review & Editing, Supervision, Funding acquisition. H.J.: Validation, Investigation, Resources, Writing-Original Draft, Writing-Review & Editing, Visualization, Supervision, Funding acquisition. All authors have read and agreed to the published version of the manuscript.

Funding: This work was supported by the National Research Foundation of Korea (NRF) grant funded by the Korean government (MSIT) (No. NRF-2021M3H4A3A02086939), and M.I. thankfully acknowledges the Department of Science and Technology-Science and Engineering Research Board (DST-SERB), EEQ/2021/000469, dt: 2 March 2022, New Delhi, India for the financial assistance.

Institutional Review Board Statement: Not applicable.

Informed Consent Statement: Informed consent was obtained from the human urine samples involved in this study.

Data Availability Statement: Not applicable.

Conflicts of Interest: The authors declare no conflict of interest.

References

1. Dryhurst, G. *Electrochemistry of Biological Molecules*; Academic Press: New York, NY, USA, 1977.
2. Grabowska, I.; Chudy, M.; Dybko, A.; Brzozka, Z. Uric acid determination in a miniaturized flow system with dual optical detection. *Sens. Actuators B* **2008**, *130*, 508–513. [CrossRef]
3. Raj, C.R.; Ohsaka, T. Voltammetric detection of uric acid in the presence of ascorbic acid at a gold electrode modified with a self-assembled monolayer of heteroaromatic thiol. *J. Electroanal. Chem.* **2003**, *540*, 69–77.
4. Kannan, P.; John, S.A. Determination of nanomolar uric and ascorbic acids using enlarged gold nanoparticles modified electrode. *Anal. Biochem.* **2009**, *386*, 65–72. [CrossRef] [PubMed]
5. Johnson, R.J.; Kang, D.H.; Feig, D.; Kivlighn, S.; Kanellis, J.; Watanabe, S.; Tuttle, K.R.; Rodriguez-Iturbe, B.; HerreraAcosta, J.; Mazzali, M. Is there a pathogenetic role for uric acid in hypertension and cardiovascular and renal disease? *Hypertension* **2003**, *41*, 1183–1190. [CrossRef] [PubMed]
6. Gagliardi, A.C.M.; Miname, M.H.; Santos, R.D. Uric acid: A marker of increased cardiovascular risk. *Atherosclerosis* **2009**, *202*, 11–17. [CrossRef]
7. Rocha, D.L.; Rocha, F.R.P. A flow-based procedure with solenoid micro-pumps for the spectrophotometric determination of uric acid in urine. *Microchem. J.* **2010**, *94*, 53–59. [CrossRef]
8. Buhimschi, C.S.; Norwitz, E.R.; Funai, E.; Richman, S.; Guller, S.; Lockwood, C.J.; Buhimschi, I.A. Urinary angiogenic factors cluster hypertensive disorders and identify women with severe preeclampsia. *Am. J. Obstet. Gynecol.* **2005**, *192*, 734–741. [CrossRef]
9. Moccia, M.; Lanzillo, R.; Palladino, R.; Russo, C.; Carotenuto, A.; Massarelli, M.; Vacca, G.; Vacchiano, V.; Nardone, A.; Triassi, M.; et al. Uric acid: A potential biomarker of multiple sclerosis and of its disability. *Clin. Chem. Lab. Med.* **2015**, *53*, 753–759. [CrossRef]
10. Aafria, S.; Kumari, P.; Sharma, S.; Yadav, S.; Batra, B.; Rana, J.S.; Sharma, M. Electrochemical biosensing of uric acid: A review. *Microchem. J.* **2022**, *182*, 107945. [CrossRef]
11. Javier, E.L.V.; Ronei, J.P. A portable SERS method for the determination of uric acid using a paper-based substrate and multivariate curve resolution. *Analyst* **2016**, *141*, 1966–1972.
12. Zhao, S.; Wang, J.; Ye, F.; Liu, Y.M. Determination of uric acid in human urine and serum by capillary electrophoresis with chemiluminescence detection. *Anal. Biochem.* **2008**, *378*, 127–131. [CrossRef] [PubMed]
13. Chen, S.; Zheng, H.; Wang, J.; Hou, J.; He, Q.; Liu, H.; Xiong, C.; Kong, X.; Nie, Z. Carbon nanodots as a matrix for the analysis of low-molecular-weight molecules in both positive- and negative-ion matrix-assisted laser desorption/ionization time-of-flight mass spectrometry and quantification of glucose and uric acid in real sample. *Anal. Chem.* **2013**, *85*, 6646–6652. [CrossRef]
14. Chen, Y.; Ji, P.; Ma, G.; Song, Z.; Tang, B.Q.; Li, T. Simultaneous determination of cellular adenosine nucleotides, malondialdehyde, and uric acid using HPLC. *Biomed. Chromatogr.* **2021**, *35*, e5156. [CrossRef]
15. Bera, R.K.; Anoop, A.; Raj, C.R. Enzyme-free colorimetric assay of serum uric acid. *Chem. Commun.* **2011**, *47*, 11498–11500. [CrossRef] [PubMed]
16. Wang, X.Y.; Zhu, G.B.; Cao, W.D.; Liu, Z.J.; Pan, C.G.; Hu, W.J.; Zhao, W.Y.; Sun, J.F. A novel ratiometric fluorescent probe for the detection of uric acid in human blood based on H_2O_2-mediated fluorescence quenching of gold/silver nanoclusters. *Talanta* **2019**, *191*, 46–53. [CrossRef] [PubMed]
17. Seok, J.S.; Ju, H. Plasmonic optical biosensors for detecting c-reactive protein: A review. *Micromachines* **2020**, *11*, 895. [CrossRef] [PubMed]
18. Kaushal, S.; Nanda, S.S.; Yi, D.K.; Ju, H. Effects of aspect ratio heterogeneity of an assembly of gold nanorod on localized surface plasmon resonance. *J. Phys. Chem. Lett.* **2020**, *11*, 5972–5979. [CrossRef]
19. Rajamanikandan, R.; Sasikumar, K.; Kosame, S.; Ju, H. Optical Sensing of Toxic Cyanide Anions Using Noble Metal Nanomaterials. *Nanomaterials* **2023**, *13*, 290. [CrossRef]
20. Tran NH, T.; Trinh KT, L.; Lee, J.H.; Yoon, W.J.; Ju, H. Reproducible Enhancement of Fluorescence by Bimetal Mediated Surface Plasmon Coupled Emission for Highly Sensitive Quantitative Diagnosis of Double-Stranded DNA. *Small* **2018**, *14*, 1801385. [CrossRef]

21. Tran NH, T.; Phan, T.B.; Nguyen, T.T.; Ju, H. Coupling of silver nanoparticle-conjugated fluorescent dyes into optical fiber modes for enhanced signal-to-noise ratio. *Biosens. Bioelectron.* **2021**, *176*, 112900. [CrossRef]
22. Tran, V.T.; Ju, H. Fluorescence Based on Surface Plasmon Coupled Emission for Ultrahigh Sensitivity Immunoassay of Cardiac Troponin I. *Biomedicines* **2021**, *9*, 448. [CrossRef] [PubMed]
23. Tran NH, T.; Trinh KT, L.; Lee, J.H.; Yoon, W.J.; Ju, H. Fluorescence enhancement using bimetal surface plasmon-coupled emission from 5-carboxyfluorescein (FAM). *Micromachines* **2018**, *9*, 460. [CrossRef] [PubMed]
24. Rajamanikandan, R.; Ilanchelian, M. Protein-localized bright-red fluorescent gold nanoclusters as cyanide-selective colorimetric and fluorometric nanoprobes. *ACS Omega* **2018**, *10*, 14111–14118. [CrossRef] [PubMed]
25. Zhang, L.; Wang, E. Metal nanoclusters: New fluorescent probes for sensors and bioimaging. *Nano Today* **2014**, *9*, 132–157. [CrossRef]
26. Díez, I.; Ras, R.H. Fluorescent silver nanoclusters. *Nanoscale* **2011**, *3*, 1963–1970. [CrossRef]
27. Choi, S.; Dickson, R.M.; Yu, J. Developing luminescent silver nanodots for biological applications. *Chem. Soc. Rev.* **2012**, *41*, 1867–1891. [CrossRef]
28. Lu, Y.; Wei, W.; Chen, W. Copper nanoclusters: Synthesis, characterization and properties. *Chin. Sci. Bull.* **2012**, *57*, 41–47. [CrossRef]
29. Singh, A.; Kaur, S.; Kaur, A.; Aree, T.; Kaur, N.; Singh, N.; Bakshi, M.S. Aqueous-Phase Synthesis of Copper Nanoparticles Using Organic Nanoparticles: Application of Assembly in Detection of Cr^{3+}. *ACS Sustain. Chem. Eng.* **2014**, *2*, 982–990. [CrossRef]
30. Ma, S.-Y.; Yeh, Y.-C. One-step synthesis of water-soluble fluorescent copper nanoparticles for label-free detection of manganese ions. *Anal. Methods* **2015**, *7*, 6475–6478. [CrossRef]
31. Wang, Z.; Chen, B.; Rogach, A.L. Synthesis, optical properties and applications of light-emitting copper nanoclusters. *Nanoscale Horiz.* **2017**, *2*, 135–146. [CrossRef]
32. Shekhar, S.; Mahato, P.; Yadav, R.; Verma, S.D.; Mukherjee, S. White light generation through l-ascorbic acid-templated thermoresponsive copper nanoclusters. *ACS Sustain. Chem. Eng.* **2022**, *10*, 1379–1389. [CrossRef]
33. Liu, X.; Astruc, D. Atomically precise copper nanoclusters and their applications. *Coord. Chem. Rev.* **2018**, *359*, 112–126. [CrossRef]
34. Shahsavari, S.; Hadian-Ghazvini, S.; Saboor, F.H.; Oskouie, I.M.; Hasany, M.; Simchi, A.; Rogach, A.L. Ligand functionalized copper nanoclusters for versatile applications in catalysis, sensing, bioimaging, and optoelectronics. *Mater. Chem. Front.* **2019**, *3*, 2326–2356. [CrossRef]
35. Rajamanikandan, R.; Azaad, B.; Kumar, L.S.; Ilanchelian, M. Glutathione functionalized copper nanoclusters as a fluorescence platform for specific biosensing of cysteine and application in cellular imaging. *Microchem. J.* **2020**, *158*, 105253. [CrossRef]
36. Jia, X.; Yang, X.; Li, J.; Li, D.; Wang, E. Stable Cu nanoclusters: From an aggregation-induced emission mechanism to biosensing and catalytic applications. *Chem. Commun.* **2014**, *50*, 237–239. [CrossRef] [PubMed]
37. Rajamanikandan, R.; Ilanchelian, M. Protein-protected red emittive copper nanoclusters as a fluorometric probe for highly sensitive biosensing of creatinine. *Anal. Methods* **2018**, *10*, 3666–3674. [CrossRef]
38. Wang, Z.; Susha, A.S.; Chen, B.; Reckmeier, C.; Tomanec, O.; Zboril, R.; Zhong, H.; Rogach, A.L. Poly(vinylpyrrolidone) supported copper nanoclusters: Glutathione enhanced blue photoluminescence for application in phosphor converted light emitting devices. *Nanoscale* **2016**, *8*, 7197–7202. [CrossRef]
39. Rajamanikandan, R.; Ilanchelian, M. Fluorescence sensing approach for high specific detection of 2,4,6-trinitrophenol using bright cyan blue color-emittive poly(vinylpyrrolidone)-supported copper nanoclusters as a fluorophore. *ACS Omega* **2018**, *3*, 18251–18257. [CrossRef]
40. Rajamanikandan, R.; Ilanchelian, M. Simple smartphone merged rapid colorimetric platform for the environmental monitoring of toxic sulfide ions by cysteine functionalized silver nanoparticles. *Microchem. J.* **2022**, *174*, 107071. [CrossRef]
41. Zhou, T.; Yao, Q.; Zhao, T.; Chen, X. One-pot synthesis of fluorescent DHLA-stabilized Cu nanoclusters for the determination of H_2O_2. *Talanta* **2015**, *141*, 80–85. [CrossRef]
42. Lee, Y.D.; Lim, C.K.; Singh, A.; Koh, J.; Kim, J.; Kwon, I.C.; Kim, S. Dye/peroxalate aggregated nanoparticles with enhanced and tunable chemiluminescence for biomedical imaging of hydrogen peroxide. *ACS Nano* **2012**, *6*, 6759–6766. [CrossRef] [PubMed]
43. Ling, Y.; Zhang, N.; Qu, F.; Wen, T.; Gao, Z.F.; Li, N.B.; Luo, H.Q. Fluorescent detection of hydrogen peroxide and glucose with polyethyleneimine-templated Cu nanoclusters. *Spectrochim. Acta Part A Mol. Biomol. Spectrosc.* **2014**, *118*, 315–320. [CrossRef] [PubMed]
44. Leed, M.G.D.; Wolkow, N.; Pham, D.M.; Daniel, C.L.; Dunaief, J.L.; Franz, K.J. Prochelators Triggered by Hydrogen Peroxide Provide Hexadentate Iron Coordination to Impede Oxidative Stress. *J. Inorg. Biochem.* **2011**, *105*, 1161–1172. [CrossRef] [PubMed]
45. Jin, L.; Shang, L.; Guo, S.; Fang, Y.; Wen, D.; Wang, L.; Yin, J.; Dong, S. Biomolecule- stabilized Au nanoclusters as a fluorescence probe for sensitive detection of glucose. *Biosens. Bioelectron.* **2011**, *26*, 1965–1969. [CrossRef] [PubMed]
46. Lakowicz, J.R. (Ed.) *Principles of Fluorescence Spectroscopy*; Springer US: Boston, MA, USA, 2006.
47. Rajan, D.; Rajamanikandan, R.; Ilanchelian, M. Investigating the biophysical interaction of serum albumins-gold nanorods using hybrid spectroscopic and computational approaches with the intent of enhancing cytotoxicity efficiency of targeted drug delivery. *J. Mol. Liq.* **2023**, *377*, 121541. [CrossRef]
48. Park, J.S.; Wilson, J.N.; Hardcastle, K.I.; Bunz, U.H.; Srinivasarao, M. Reduced fluorescence quenching of cyclodextrin− acetylene dye rotaxanes. *J. Am. Chem. Soc.* **2006**, *128*, 7714–7715. [CrossRef]

49. Shiang, Y.-C.; Huang, C.-C.; Chang, H.-T. Gold nanodot-based luminescent sensor for the detection of hydrogen peroxide and glucose. *Chem. Commun.* **2009**, *2009*, 3437–3439. [CrossRef]
50. Wang, J.; Chang, Y.; Wu, W.B.; Zhang, P.; Lie, S.Q.; Huang, C.Z. Label-free and selective sensing of uric acid with gold nanoclusters as optical probe. *Talanta* **2016**, *152*, 314–320. [CrossRef]
51. Zhao, Y.; Yang, X.; Lu, W.; Liao, H.; Liao, F. Uricase based methods for determination of uric acid in serum. *Microchim. Acta* **2009**, *164*, 1–6. [CrossRef]
52. Kong, R.M.; Yang, A.; Wang, Q.; Wang, Y.; Ma, L.; Qu, F. Uricase based fluorometric determination of uric acid based on the use of graphene quantum dot@silver core-shell nanocomposites. *Microchim. Acta* **2018**, *185*, 63. [CrossRef]
53. Wang, H.; Lu, Q.; Hou, Y.; Liu, Y.; Zhang, Y. High fluorescence S, N co-doped carbon dots as an ultra-sensitive fluorescent probe for the determination of uric acid. *Talanta* **2016**, *155*, 62–69. [CrossRef] [PubMed]
54. Liu, M.; He, Y.; Zhou, J.; Ge, Y.; Zhou, J.; Song, G. A "naked-eye" colorimetric and ratiometric fluorescence probe for uric acid based on Ti3C2 MXene quantum dots. *Anal. Chim. Acta* **2020**, *1103*, 134–142. [CrossRef] [PubMed]
55. Li, F.; Rui, J.; Yan, Z.; Qiu, P.; Tang, X. A highly sensitive dual-read assay using nitrogen-doped carbon dots for the quantitation of uric acid in human serum and urine samples. *Microchim. Acta* **2021**, *188*, 311. [CrossRef] [PubMed]
56. Azmi, N.E.; Ramli, N.I.; Abdullah, J.; Abdul Hamid, M.A.; Sidek, H.; Abd Rahman, S.; Ariffin, N.; Yusof, N.A. A simple and sensitive fluorescence-based biosensor for the determination of uric acid using H_2O_2-sensitive quantum dots/dual enzymes. *Biosens. Bioelectron.* **2015**, *67*, 129–133. [CrossRef]
57. Liu, Y.; Li, H.; Guo, B.; Wei, L.; Chen, B.; Zhang, Y. Gold nanoclusters as switch-off fluorescent probe for detection of uric acid based on the inner filter effect of hydrogen peroxide-mediated enlargement of gold nanoparticles. *Biosens. Bioelectron.* **2017**, *91*, 734–740. [CrossRef] [PubMed]
58. Azmia, N.E.; Rashid, A.H.A.; Abdullah, J.; Yusof, N.A.; Sidek, H. Fluorescence biosensor based on encapsulated quantum dots/enzymes/sol-gel for non-invasive detection of uric acid. *J. Lumin.* **2018**, *202*, 309–315. [CrossRef]
59. Jin, D.; Seo, M.-H.; Huy, B.T.; Pham, Q.-T.; Conte, M.L.; Thangadurai, D.; Lee, Y.-I. Quantitative determination of uric acid using CdTe nanoparticles as fluorescence probes. *Biosens. Bioelectron.* **2016**, *77*, 359–365. [CrossRef]
60. Ma, C.; Li, P.; Xia, L.; Qu, F.; Kong, R.-M.; Song, Z.-L. A novel ratiometric fluorescence nanoprobe for sensitive determination of uric acid based on CD@ZIF-CuNC nanocomposites. *Microchim. Acta* **2021**, *188*, 259. [CrossRef]